Ref.TH.2801-CERN

ON LARGE ANGLE MESON-BARYON ELASTIC SCATTERING

G. Preparata
CERN -- Geneva
and
Istituto di Fisica dell'Università di Bari

and

J. Soffer *)
CERN -- Geneva

ABSTRACT

We have extended a recent calculation of the nucleon-nucleon large angle elastic scattering amplitudes, to the meson-baryon case. Comparison with the available experimental information indicates that we have an accurate description of hadronic interactions at short distances.

---

*) On leave from Centre de Physique Théorique, CNRS, Marseille, France.

Ref.TH.2801-CERN
19 December 1979

In a previous letter[1] we have drawn the attention to the fact that there exists a theoretical approach which is powerful, predictive and simple enough so that several very interesting problems of hadronic physics can be solved. There we have shown that features in both spin and flavour dependence in large angle nucleon-nucleon scattering were a natural consequence of a few very simple ideas which form the basis of the mentioned theoretical approach, which has scored a remarkable success exactly when the popular and generally accepted descriptions of short distance behaviour in hadronic physics (like the CIM[2]) appear to have serious problems.

In this letter we want to apply the same ideas to the description of large angle meson-baryon scattering. It will be seen that, again, our calculations, are in remarkable agreement with very recent data obtained at CERN[3),4)].

When dealing with meson-baryon scattering at large angle there are two classes of contributions which we must consider: the meson-exchange and the baryon-exchange diagrams. The meson-exchange diagrams, whose topology we label (a,b), according to the meson exchange channel a and the $q\bar{q}$ scattering channel b, are reported in Fig. 1 (a). The baryon-exchange diagrams, labelled (α,β), according to the baryon-exchange channel α and the $q\bar{q}$ scattering channel β, appear in Fig. 2(b).

The calculation*) of the diagrams of Fig. 1(a), follows very closely Ref. 1), with the only difference that the meson overlap function appearing in the upper part of the diagrams, is calculated to be (a,b are flavour indices, while i,j are spin indices, M,M' are SU(3) matrices, θ is the CM scattering angle)

$$V(M,M',\theta)^{bj}_{ai} = (MM'^{+})^{b}_{a}\left[\cos\theta/2\,\delta^{j}_{i} + (i\sigma_2)^{j}_{i}\sin\theta/2\right] \qquad (1)$$

for the (t,u) and the (u,t) topologies, whereas for the (s,t) topology we should take the Hermitian conjugate of (1). For each meson and each topology the two helicity amplitudes f_+ (helicity non-flip) and f_- (helicity flip) can be written as

$$f^{(a,b)}_{\pm,mp}(s,\theta) = g^{(a,b)}(s,\theta)\; A^{(a,b)}_{\pm,mp}(\theta) \qquad (2)$$

---

*) A detailed account of the whole calculation shall be presented elsewhere.

where

$$g^{(s,t)}(s,\theta) = g^{(u,t)}(s,\theta) = \frac{1}{s^{7/2}} \log\left(\frac{s}{m_0^2}\right) \frac{1}{(1-\cos\theta)^3} \qquad (2')$$

$$g^{(t,u)}(s,\theta) = \frac{1}{s^{7/2}} \log\left(\frac{s}{m_0^2}\right) \frac{1}{(\sin\theta)^3} \qquad (2'')$$

m_0^2 is a constant and $A^{(a,b)}_{\pm,Mp}(\theta)$ are given in Tables Ia and Ib.

In order to calculate the diagrams of Fig. 1(b), we must first evaluate the high energy limit of the 3q Green's function, and then sort out the behaviour of MBB_n overlap integrals. This can be done without any big difficulty. The high energy limit of the 3q Green's function can be evaluated in a manner completely similar to the $q\bar{q}$ Green's function, while the MBB_n overlap is easily evaluated from the baryon wave function's given in Ref. 6). Writing, with obvious notation:

$$f^{(\alpha,\beta)}_{\pm,Mp}(s,\theta) = \gamma^{(\alpha,\beta)}(s,\theta)\; B^{(\alpha,\beta)}_{\pm,Mp}(\theta) \qquad (3)$$

we get

$$\gamma^{(s,t)}(s,\theta) = \left(\log\left(\frac{s}{m_0^2}\right) - i\pi\right) \frac{1}{s^{7/2}} \frac{1}{(1-\cos\theta)^{3/2}}$$

$$\gamma^{(u,t)}(s,\theta) = -\log\left(\frac{s}{m_0^2}\right) \frac{1}{s^{7/2}} \frac{2}{(1+\cos\theta)} \frac{1}{(1-\cos\theta)^{3/2}} \qquad (3')$$

and the values of $B^{(\alpha,\beta)}_{\pm,Mp}(\theta)$ are given in Tables IIa and IIb. From our definition of the amplitudes we obtain the following differential cross-section

$$\frac{d\sigma}{dt}^{(Mp)} = \frac{N}{s^2}\left\{\left|\sum_{(\alpha,\beta)} f^{(\alpha,\beta)}_{+,Mp}(s,\theta) + \lambda \sum_{(a,b)} f^{(a,b)}_{+,Mp}(s,\theta)\right|^2 \right. \qquad (4)$$

$$\left. + \left|\sum_{(\alpha,\beta)} f^{(\alpha,\beta)}_{-,Mp}(s,\theta) + \lambda \sum_{(a,b)} f^{(a,b)}_{-,Mp}(s,\theta)\right|^2\right\}$$

$$\xrightarrow[s\to\infty]{} \log^2\left(\frac{s}{m_0^2}\right) \frac{1}{s^9} F^{Mp}(\theta) \qquad (4')$$

where, except for an over-all normalization factor N, λ and m_0^2 are the only free paremeters appearing in our calculation. Notice the "scaling law" (4') which, modulo logs, is characterized by an s^{-9} power instead of an s^{-8}, which one encounters in "power counting" models like CIM[2]. Fixing $\lambda = 1/20$, $m_0^2 = 2\ GeV^2$ and the normalization so as to fit $\pi^+ p|_{60^0}$ at $p_{Lab} = 10$ GeV/c, the curves we obtain for $\pi^{\pm} p$ and $K^{\pm} p$ for $p_{Lab} = 10,20$ and 30 GeV/c are reported in Fig. 2. The comparison with the data at the highest energy presently available, Refs 3),4),7) is carried out in Fig. 3.

We know of no other theoretical proposal which is able to reproduce the experimental observations.

Table Ia

$A^{(\alpha,\beta)}_{+,Mp}(\theta)$

Mp \ (a,b)	(t,u)	(s,t)	(u,t)
π^+p	$\cos\theta/2(3 + \cos\theta)(5 + \cos\theta)$	$\cos\theta/2(2 + \cos\theta)(5 + 2\cos\theta)$ - $- \sin\theta/2(3 - 2\cos\theta)\sin\theta$	$\cos\theta/2(\frac{11 + 3\cos\theta}{2})(2 + \cos\theta)$ - $- \sin\theta/2\sin\theta(\frac{3 - 5\cos\theta}{2})$
π^-p	$\cos\theta/2(3 + \cos\theta)(1 + 2\cos\theta)$	same as π^+p	same as π^+p
K^+p	same as π^+p	same as π^+p	same as π^+p
K^-p	0	same as π^+p	same as π^+p

Table Ib

$A^{(a,b)}_{-,Mp}(\theta)$

Mp \ (a,b)	(t,u)	(s,t)	(u,t)
π^+p	$\cos\theta/2(3 + \cos\theta)\ \sin\theta$	$\cos\theta/2(5 + 2\cos\theta)\ \sin\theta +$ $+ \sin\theta/2(3 - 2\cos\theta)(2 - \cos\theta)$	$\cos\theta/2(\frac{11 + 3\cos\theta}{2})\ \sin\theta +$ $+ \sin\theta/2(2 - \cos\theta)(\frac{3 - 5\cos\theta}{2})$
π^-p	$\cos\theta/2\ 2(3 + \cos\theta)2\sin\theta$	same as π^+p	same as π^+p
K^+p	same as π^+p	same as π^+p	same as π^+p
K^-p	0	same as π^+p	same as π^+p

Table IIa

$B^{(\alpha,\beta)}_{+,\,Mp}(\theta)$

Mp \ (α,β)	(s,t)	(u,t)
π^+p	$\cos\theta/2(1 + 2\cos\theta) + \sin\theta/2\ 2\sin\theta$	$\cos\theta/2(5 + \cos\theta) - \sin\theta\ \sin\theta/2$
π^-p	$\cos\theta/2(5 + \cos\theta) + \sin\theta/2\ \sin\theta$	$(1 + 2\cos\theta)\cos\theta/2 - 2\sin\theta/2\ \sin\theta$
K^+p	0	same as π^+p
K^-p	same as π^-p	0

Table IIb

$B^{(\alpha,\beta)}_{-,\,Mp}(\theta)$

Mp \ (α,β)	(s,t)	(u,t)
π^+p	$2\cos\theta/2\ \sin\theta - \sin\theta/2(1 - 2\cos\theta)$	$\cos\theta/2\ \sin\theta + (5 - \cos\theta)\sin\theta/2$
π^-p	$\cos\theta/2\ \sin\theta - (5 - \cos\theta)\ \sin\theta/2$	$2\cos\theta/2\ \sin\theta + \sin\theta/2(1 - 2\cos\theta)$
K^+p	0	same as π^+p
K^-p	same as π^-p	0

REFERENCES

1) G. Preparata and J. Soffer, Phys. Lett. 86B (1979) 304.

2) J.F. Gunion et al., Phys. Rev. D8 (1973) 287;
D. Sivers et al., Phys. Reports 23C (1976) 1.

3) C. Baglin et al., Phys. Rev. Letters 40 (1978) 425.

4) CERN, Annecy (LAPP), Genova, Copenhagen, Oslo, London (U.C.) collaboration
CERN/EP-79-75 (July 1979) and forthcoming paper submitted to Phys. Lett. B.

5) G. Preparata, Nucl. Phys. B122 (1977) 29.

6) G. Preparata and K. Szegö, Nuovo Cim. 47A (1978) 303.

7) D.P. Owen et al., Phys. Rev. 181 (1969) 1794.

TABLE CAPTIONS

Table I : The functions $A^{(a,b)}_{+,Mp}(\theta)$ (a) and $A^{(a,b)}_{-,\mu p}(\theta)$ (b), as defined in (2).

Table II : The functions $B^{(\alpha,\beta)}_{+,Mp}(\theta)$ (a), and $B^{(\alpha,\beta)}_{-,Mp}(\theta)$ (b), as defined in (3).

FIGURE CAPTIONS

Fig. 1 : The different topologies:
a) the relevant meson-exchange diagrams;
b) the relevant baryon-exchange diagrams.

Fig. 2 : Our predictions for large angle differential cross-sections for $\pi^{\pm}p$, $K^{\pm}p$ elastic scattering at p_{lab} = 10,20 and 30 GeV/c.

Fig. 3 : a) Comparison of our predictions for $\pi^{+}p$ with the data at p_{lab} = 10 GeV/c [Ref. 3)] and p_{lab} = 20 GeV/c [Ref. 4)];
b) same for $\pi^{-}p$ with the data at p_{lab} = 9.71 and 9.84 GeV/c [Ref. 7)] and p_{lab} = 20 and 30 GeV/c [Ref. 4)].

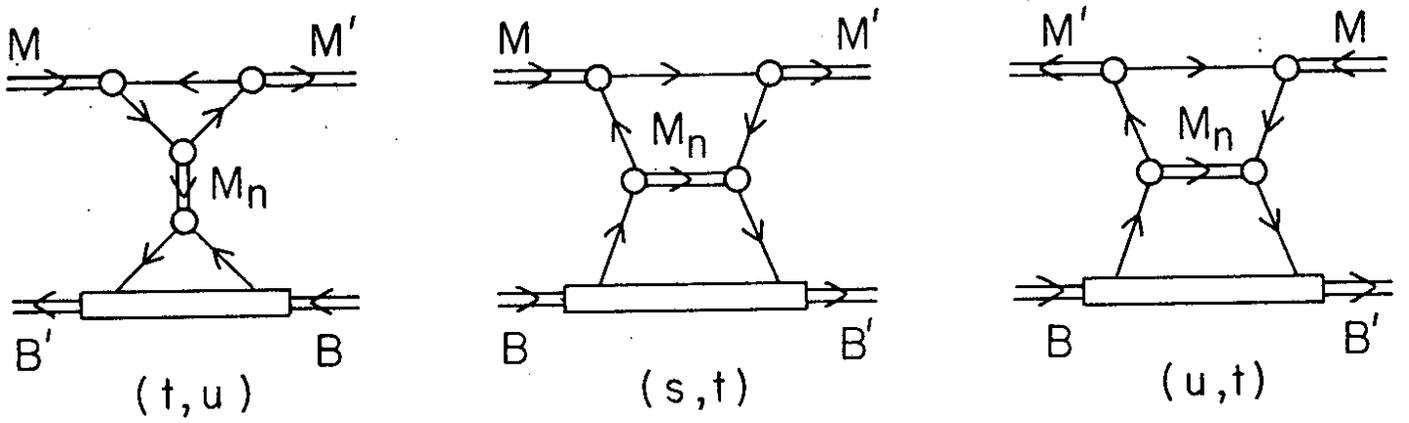

FIG. 1

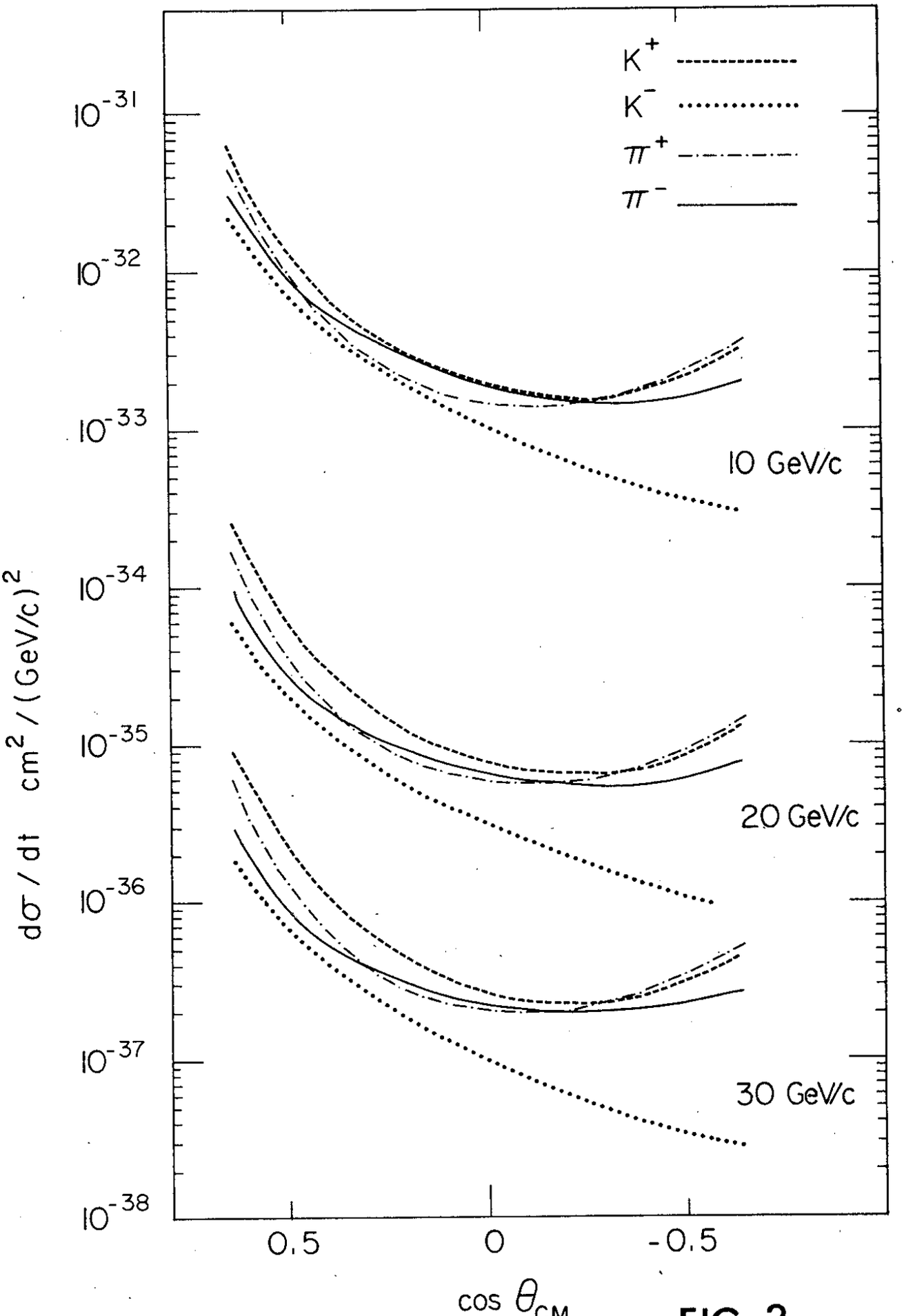
K^+
K^-
π^+
π^-
10^{-31}
10^{-32}
10^{-33}
10^{-34}
10^{-35}
10^{-36}
10^{-37}
10^{-38}
10 GeV/c
20 GeV/c
30 GeV/c
$d\sigma / dt \quad cm^2 / (GeV/c)^2$
0.5
0
-0.5
$\cos \theta_{CM}$

FIG. 2

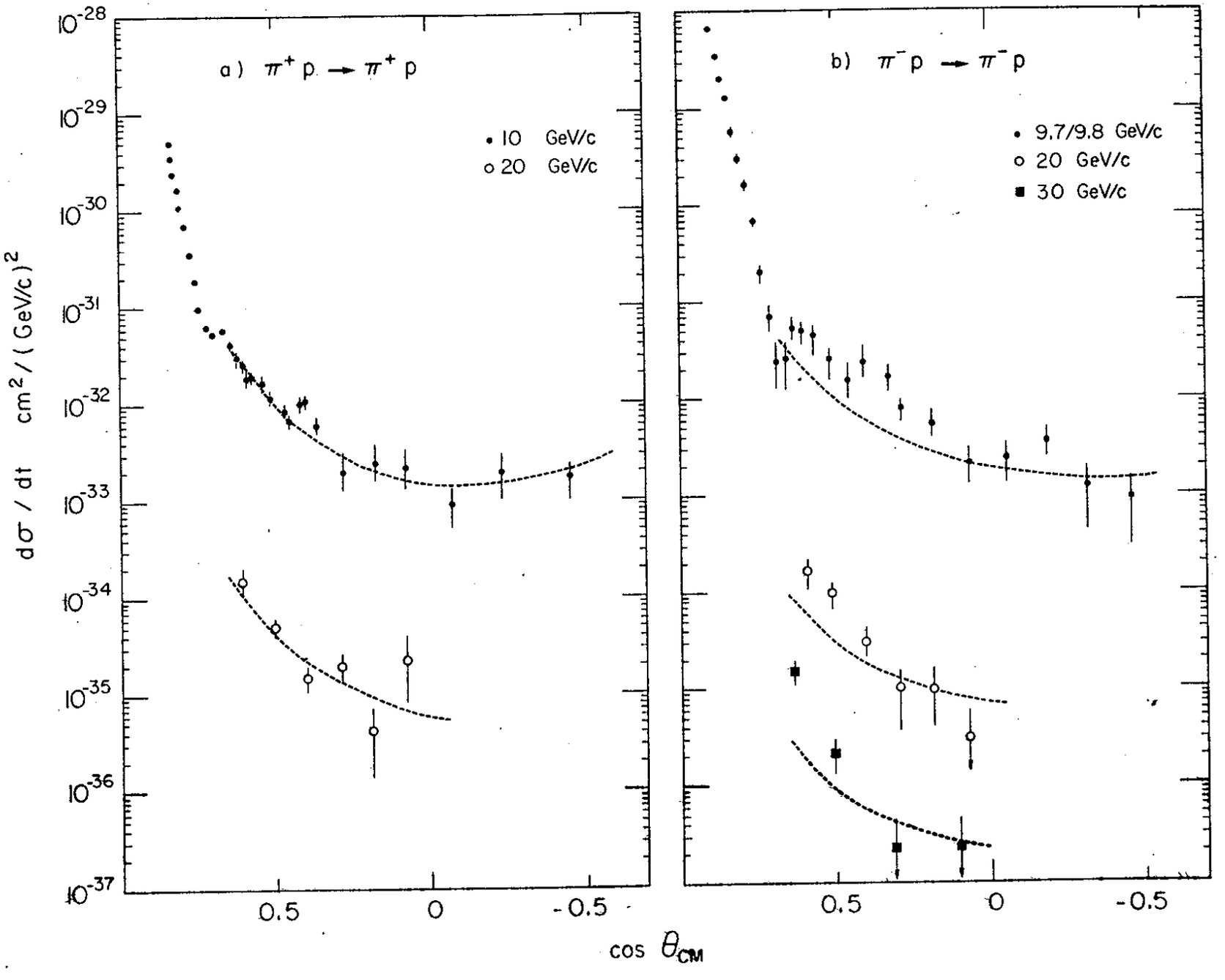
a) $\pi^+ p \rightarrow \pi^+ p$
• 10 GeV/c
o 20 GeV/c
b) $\pi^- p \rightarrow \pi^- p$
• 9.7/9.8 GeV/c
o 20 GeV/c
■ 30 GeV/c
$d\sigma / dt$ cm^2 / (GeV/c)^2
10^{-28}
10^{-29}
10^{-30}
10^{-31}
10^{-32}
10^{-33}
10^{-34}
10^{-35}
10^{-36}
10^{-37}
0.5
0
-0.5
cos θ_{CM}

FIG. 3